Journal of Controlled Release 258 (2017) 56–66

Contents lists available at ScienceDirect

Journal of Controlled Release

journal homepage: www.elsevier.com/locate/jconrel

cRGD peptide-installed epirubicin-loaded polymeric micelles for effective targeted therapy against brain tumors

S. Quader[a], X. Liu[a], Y. Chen[b], P. Mi[a], T. Chida[b], T. Ishii[b], Y. Miura[c], N. Nishiyama[d], H. Cabral[b], K. Kataoka[a,e,*]

[a] Innovation Center of Nanomedicine, Kawasaki Institute of Industrial Promotion, 3-25-14 Tonomachi, Kawasaki-ku, Kawasaki 212-0821, Japan
[b] Department of Bioengineering, Graduate School of Engineering, The University of Tokyo, 7-3-1 Hongo, Bunkyo-ku, Tokyo 113-8656, Japan
[c] Center for Disease Biology and Integrative Medicine, Graduate School of Medicine, The University of Tokyo, 7-3-1 Hongo, Bunkyo-ku, Tokyo 113-0033, Japan
[d] Laboratory for Chemistry and Life Science, Institute of Innovative Research, Tokyo Institute of Technology, R1-11, 4259 Nagatsuta, Midori-ku, Yokohama 226-8503, Japan
[e] Policy Alternatives Research Institute, The University of Tokyo, 7-3-1 Hongo, Bunkyo-ku, Tokyo 113-1709, Japan

ARTICLE INFO

Keywords:
Polymeric micelle
pH-sensitivity
Epirubicin
Brain tumor
Targeted therapy

ABSTRACT

Current therapeutic strategies against glioblastoma multiforme (GBM) are futile mainly because of the poor access of drugs into malignant tissues, which is hindered by the tight blood-brain tumor barrier in the GBM vasculature. Nanomedicines have shown potential for circumventing the vascular barriers of GBM, particularly by targeting markers on the luminal side of endothelial cells in the blood vessels of GBM for achieving effective and selective translocation into the tumor. Thus, as the αvβ3 and αvβ5 integrins overexpressed on the endothelial cells of GBM can be targeted by cyclic-Arg-Gly-Asp (cRGD) peptide, herein, we developed cRGD-installed micellar nanomedicines loading epirubicin, the potent antiglioblastoma agent, through a pH-sensitive hydrazone-bond for effective treatment of GBM. These cRGD-installed epirubicin-loaded polymeric micelles (cRGD-Epi/m) achieved faster and higher penetration into U87MG cell-derived 3D-spheroids than the micelles without cRGD, conceivably through a cRGD-integrin mediated pathway. *In vivo*, the cRGD-installed micelles effectively suppressed the growth of an orthotopic GBM model by delivering high levels of epirubicin throughout the tumor tissue. These results indicate significant prospects for cRGD-Epi/m as an effective and translationable treatment against GBM.

1. Introduction

Glioblastoma multiforme (GBM) represents the most frequent and deadliest of astroglial tumors, with < 5% of patients with GBM surviving longer than 3 years [1,2]. The most dominant factors for this poor prognosis of GBM are its high invasive [3] and angiogenic [4] character, the inherent resistance of GBM to traditional therapies [2] and the presence of the blood-brain tumor barrier (BBTB) in the vasculature of GBM, which limits the penetration and accumulation of drugs [5,6]. The current standard treatment of GBM consists of maximal surgical resection followed by radiotherapy (RT) with concomitant and adjuvant chemotherapy with temozolomide (TMZ) [7]. While TMZ has made an impact on survival (median survival improved from 12.1 months with only RT to 14.6 months with RT plus TMZ); tumor recurrence and TMZ resistance remain major challenges [7,8]. Thus, effective chemotherapeutic approaches against GBM should be designed for overcoming the vascular barriers and being sufficiently potent to eradicate cancer cells.

Nanomedicines could improve the efficiency of chemotherapies by selectively delivering drugs to tumors [9–11]. While the preferential accumulation of nanomedicines in solid tumors is mediated by the enhanced permeability of the malignant vasculature [12], nanomedicines targeting GBM should be modified with ligands facilitating their translocation from the vasculature into the brain tumors [13,14], as the BBTB restricts their extravasation. Among nanomedicines with potential for clinical translation, drug-loaded polymeric micelles have demonstrated significant tumor targeting in both pre-clinical and clinical trials [15,16], and the modification of their surface with cyclic Arg-Gly-Asp (cRGD) peptides, which preferentially binds to αvβ3 and αvβ5 integrins [17–20] overexpressed in tumor neovasculature and tumor cells [21], including GBM cells [22–24], could facilitate their transcellular transport into a GBM model [25]. Thus, installation of cRGD peptides on clinically evaluated polymeric micelles incorporating potent drugs against GBM cells could provide substantial therapeutic

* Corresponding author at: Innovation Center of Nanomedicine, Kawasaki Institute of Industrial Promotion, 3-25-14 Tonomachi, Kawasaki-ku, Kawasaki 212-0821, Japan.
E-mail address: k-kataoka@kawasaki-net.ne.jp (K. Kataoka).

http://dx.doi.org/10.1016/j.jconrel.2017.04.033
Received 29 December 2016; Received in revised form 12 April 2017; Accepted 24 April 2017
Available online 05 May 2017

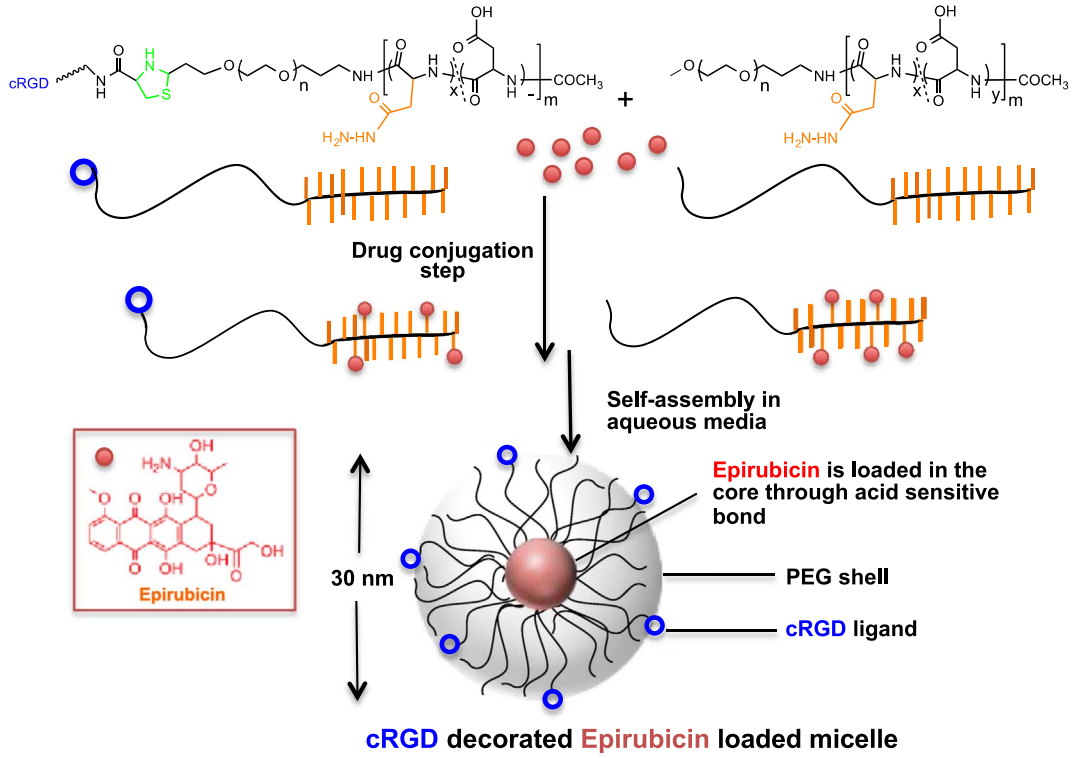

Fig. 1. Preparation of cRGD-peptide installed epirubicin-loaded polymeric micelles from a mixture (1:3) of cRGD-poly(ethylene glycol)-*b*-poly(hidrazinyl-aspartamide) and MeO-poly (ethylene glycol)-*b*-poly (hidrazinyl-aspartamide) polymer.

improvement and meet the urgent clinical needs.

Recently, epirubicin (Epi), an anthracycline, has been identified as one of the most potent antiglioblastoma agents from the NIH Clinical Collection (NCC) library of 446 FDA-approved drugs [26]. In fact, Epi was significantly more effective than current clinical antiglioblastoma drug TMZ [26]. However, anthracyclines fail to achieve therapeutic concentrations in brain tumors after intravenous injection due to their poor penetration through BBB/BBTB and efflux mediated by P-glycoprotein overexpressed in the endothelial cells of the BBB/BBTB [27]. Auspiciously, we have developed micellar nanomedicines loaded with Epi and their analogues by conjugating the drug to the poly(aspartic acid) segment of PEG-*b*-poly(aspartic acid) copolymers via an acid-sensitive hydrazone bond [28–30], which allows selective intracellular drug release after endocytosis. The Epi-loaded micelles (Epi/m) demonstrated low toxicity and high efficacy against several tumor models, and have now progressed into phase I human clinical trials (NC-6300; Nanocarrier Co., Ltd.) [16,29]. Herein, we have modified the surface of Epi/m with cRGD peptides aiming for effective GBM treatment (Fig. 1). Combining the pH-sensitive release mechanism with enhanced recognition and internalization by αvβ3/αvβ5 integrin targeting, these cRGD-installed Epi/m (cRGD-Epi/m) are expected to provide efficient antitumor effects against GBM tumor.

2. Materials and methods

2.1. Materials

Sources of materials for polymer synthesis and also basic cell culture reagents have already been described in our previous publication [31]. Additionally α-Acetal-ω-amino poly(ethylene glycol) (Acetal-PEG-NH_2; M_w = 12,000) was obtained from NOF Co, Inc. (Tokyo, Japan). Epirubicin was purchased from NanoCarrier (Chiba, Japan). Centrifugal filter tubes (MWCO = 30,000 Da) were purchased from Millipore Corporation. HPLC grade acetonitrile was purchased from Sigma-Aldrich Co. (St. Louis, MO). MTT in solid form was purchased from Dojindo Laboratories (Kumamoto, Japan). D-Luciferin potassium salt was bought from Promega Corporation.

2.2. Instruments related to polymer synthesis and characterization

For the description of the instruments for polymer synthesis and characterization we would like to refer to our previous publication [31].

2.3. Reversed-phase liquid chromatography instrumentation details

Reversed-phase liquid chromatography was performed at 40 °C on a Tosoh TSK-gel ODS-80TM (4.6 μm, 150 mm) with a Tosoh ODS-80TM guard cartridge (Tokyo, Japan). Detection was carried out using a Waters fluorescence detector with excitation and emission wavelengths of 488 and 560 nm, respectively.

2.4. Synthesis of Acetal-PEG-PBLA and MeO-PEG-PBLA

Acetal-poly(ethylene glycol)-*b*-poly(β-benzyl-aspartamide) (Acetal-PEG-PBLA) was synthesized using acetal-PEG-NH_2 as an initiator following a previously reported procedure [31,32]. The degree of polymerization was determined as 35 by ^{1}H NMR spectra using integral values from the $-CH_2CH_2O-$ proton peaks of PEG (MW = 12,000) and aryl (C_6H_5-) peak of PBLA block.

Similar procedure was used to prepare MeO-PEG-PBLA.

2.5. Acetylation of the terminal amine function of Acetal-PEG-PBLA

Acetylation of the terminal amine function of Acetal-PEG-PBLA was done according the literature procedure [31]. The efficiency of acetylation at the terminal amine was confirmed by ^{1}H NMR spectra using integral values from the methyl proton (2 × 3) peaks of acetal group (1.08 ppm) and acyl (CH_3CO-) peak (1.75 ppm) and two other methylene peak of the polymer (1.55 and 1.7 ppm).

Similar procedure was used to acetylate the ω-end amine function of MeO-PEG-PBLA to facilitate MeO-PEG-PBLA-Ac.

2.6. Conjugation of cRGD moiety to the Acetal-PEG-PBLA-Ac polymer

Acetal-PEG-PBLA-Ac (180 mg) was dissolved in d_6 DMSO (3 mL), followed by addition of deuterium chloride solution (120 μL of 2 N DCl, in D_2O). The resulting solution was stirred for 2 h at room temperature, and complete acetal deprotection (subsequent appearance of aldehyde peak) was confirmed by NMR. Cyclic RGD (25 mg) was added as solid followed by *N,N*-diisopropylethylamine (100 μL). The reaction mixture was stirred at room temperature for 3 h, and complete disappearance of aldehyde peak of PEG-PBLA polymer was confirmed by NMR. The reaction mixture was then dialyzed against cold-water, and freeze-dried to recover cRGD-conjugated polymer. To confirm the degree of cRGD conjugation, an aliquot of this polymer was subjected to quantitative ester-amide-exchange reaction [31,33], and NMR experiment was conducted, where the five aromatic proton peak of D-phenylalanine segment of cRGD was compared with the PEG proton peak. The other characteristic peaks from cRGD structure in the alkyl region (0.5–2.5 ppm) were also obvious in the spectra of cRGD-PEG-Poly (hydrazinyl-aspartamide)-Ac polymer.

2.7. Introduction of specific units of hydrazide function on to the PBLA block through ester-amide exchange reaction

A mixture of MeO-PEG-PBLA-Ac and cRGD-PEG-PBLA-Ac (3:1), or MeO-PEG-PBLA-Ac alone, was dissolved in anhydrous DMSO (1 mL for every 50 mg polymer) with gentle heating. After cooling to room temperature, anhydrous hydrazine (20 molar equivalent of polymer) was added. The reaction mixture was left stirring for 3 h at room temperature. The hydrazide containing polymers were recovered from the reaction mixture through $(Et)_2O$ precipitation and dried under vacuum. The number of hydrazide units within each polymer chain was quantified by acetylation as described in the literature [31].

2.8. Drug-conjugation reaction

Hydrazide polymer and epirubicin (10 molar equivalent to polymer weight) was dissolved in DMSO (1 mL for every 15 mg polymer and Epi mixture). The mixture was left stirring for 72 h at 40 °C. This solution was then directly used for micelle preparation.

2.9. Micelle Preparation

The drug-polymer conjugate in DMSO was dialyzed against MeOH for 24 h. The dialyzing medium was changed 4 times during this period; at the end of the dialysis process the dialyzing medium should remain colorless. The resulting methanolic solution of drug-polymer conjugate inside the dialysis bag was collected and evaporated in a 500 mL round bottom flask, which produced a thin film on the glass surface. Phosphate buffer saline (PBS, 10 mmol PB plus 150 mmol NaCl, pH 7.4) was then added (10 mg/mL) and the mixture was subjected to sonication for 10 min, which instantly produced micelle solution. Using centrifugal filter unit, with molecular weight cut off 30 kDa, residual free drug and free polymer was removed.

2.10. Size and PDI measurement by dynamic light scattering technique

Size and polydispersity of the micelles were determined by dynamic light scattering (DLS) technique at 25 °C (unless otherwise mentioned) using Zetasizer nano ZS (Malvern instruments, UK) at a detection angle of 173° with a green laser (532 nm) as the incident beam.

2.11. Evaluating the epirubicin content in micelle solution

Epirubicin micelle solution in PBS was diluted (200 times) using 0.1 N HCl solution. The acidified micelle solution was incubated an hour at 37 °C, to facilitate complete drug release. The sample was then subjected to RPLC analysis (isocratic mobile phase containing a mixture of ammonium formate buffer (25 mM and pH 3) and acetonitrile (70:30, v/v)) at a flow rate of 1 mL/min. The released epirubicin content of the sample was evaluated by comparing the peak area of the sample with that of a standard epirubicin solution. The calculated epirubicin content was multiplied by the dilution factor to get the actual epirubicin concentration in the micelle solution as mg/mL.

2.12. Drug release experiment

For the drug release studies, micelle solution (200 μg/mL) was diluted 10 times in different experimental buffers (PBS buffer pH 7.4, acetate buffer pH 5 and 3) and kept incubated at 37 °C for the total experimental period of 72 h. Released drug was measured directly from the micelle solution in experimental buffer using RPLC (as described above) analysis in predetermined time points.

2.13. Calculation of drug loading

A known volume of micelle solution in PBS was freeze-dried, and weight of the sample was measured. The same volume of PBS buffer solution was also freeze-dried, and the weight of the dried PBS was subtracted from the dry polymer-epirubicin conjugate including PBS to get the weight of only polymer-epirubicin conjugate. From this weight, per mL polymer weight was calculated; comparing this weight with the epirubicin concentration in micelle solution, % drug loading can be calculated according to the following equation. From the % drug loading, conjugated epirubicn units can also be calculated.

$$\%\text{Drug Loading} = \frac{\text{Epi concentration in micelle solution (mg/mL)}}{\text{Concentration of Polymer-Epi conjugate (mg/mL)}} \times 100$$

2.14. In vitro cytotoxicity

In vitro cytotoxicity of Epi and Epi micelles (Epi/m and cRGD Epi/m) was evaluated against U87MG cell line. Cells were seeded (3000 cells/well), and were cultured in appropriate medium in 96-well-plates. The cells were then exposed (for 3 h or 48 h) to free drug and micelle solution. For short time drug exposure, the cells were incubated for further 48 h after washing with fresh medium. After that, 10 μL of MTT solution (5 mg/mL) was added in each well, incubated for additional 4 h, which was followed by addition of 100 μL of solubilizing solution (10% SDS and 0.01 mol/L HCl). Absorbance (at 570 nm) was measured, after 12 hour incubation, using a Microplate Reader (Bio-Rad Model 680 (BIO-RAD, Hercules, CA).

2.15. In vitro cell internalization study in 2D layer

U87MG cells were seeded (1000 cells/well) in a glass bottom 8 well slides (Ibidi μ-slide 8 well), incubated for 24 h in a humidified atmosphere of 5% CO_2 at 37 °C and exposed with drugs and micelles. Three minutes before the predetermined time point, hoechst were added to the medium (as in 10 μL hoechst for 1 mL cell culture medium) and incubated for 3 min. Cells were then washed (3 times with PBS) and fixed with 4% paraformaldehyde (incubated for 30 min at RT). After washing the cells with fresh PBS, imaging study was performed using CLSM (LSM 880, Carl Zeiss, Oberlochen, Germany) with a Plan-Apochromate 63 ×/1.4 oil objective lens, diode laser (405 nm) for Hoechst and Ar-laser (458 nm/488 nm/514 nm) for epirubicin. ZEN2010 software was used to process the imaging data. Data was averaged from 3 samples (n = 3) containing 10–20 cells per sample.

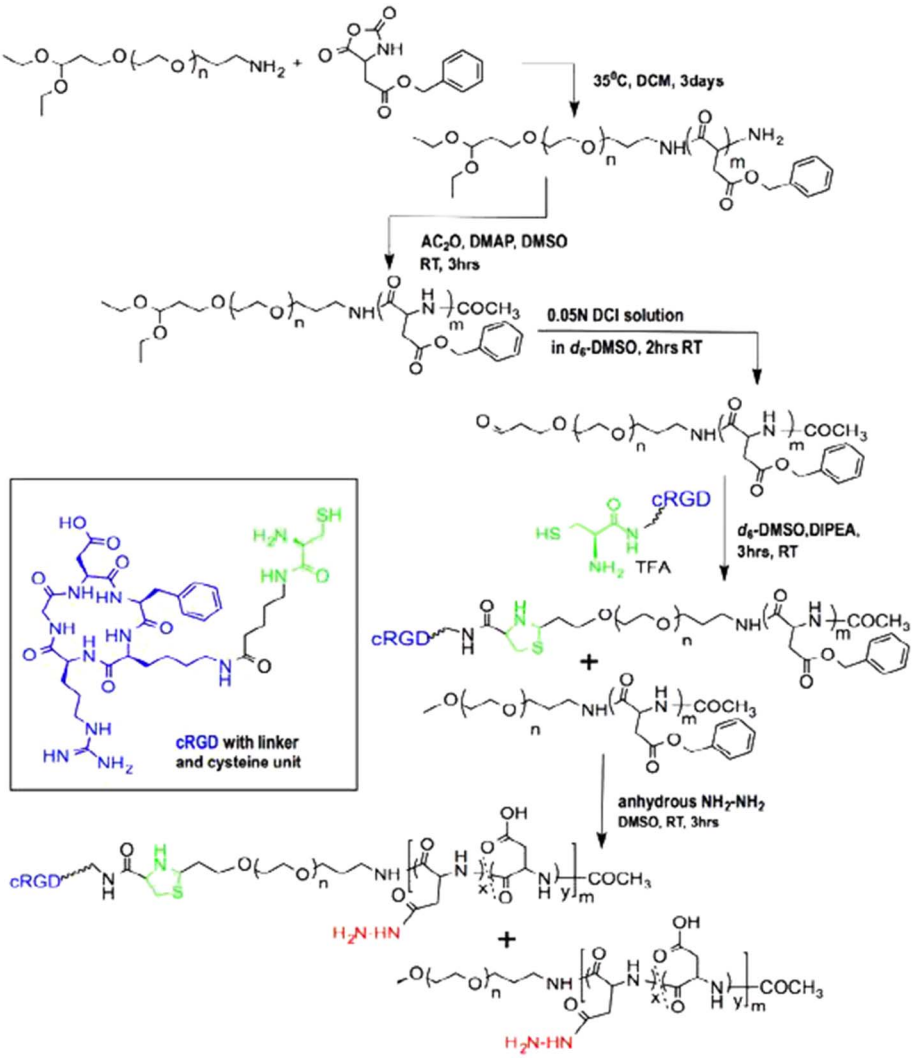

Scheme 1. Synthesis scheme of cRGD-installed poly(ethylene glycol)-*b*-poly(hydrazinyl-aspartamide).

The statistical significance of the data was determined by using unpaired Student's *t*-test. The results were considered statistically significant if *P* values were lower than 0.05.

2.16. Spheroid preparation study

U87MG cells were seeded (1000 cells/well) in U-bottomed 96-well-plates (PrimeSurface, Sumitomo Bakelite Co., Ltd.), and incubated for 24 h in a humidified atmosphere of 5% CO_2 at 37 °C. Within this time, 3D cell aggregates of diameter around 300 μm were spontaneously formed. The 3D cell aggregates were then exposed (for 3, 6 and 24 h) to Epi, Epi/m or cRGD-Epi/m micelle solution (0.3 μg/mL epirubicin concentration). The spheroids were then washed with PBS, fixed with 4% paraformaldehyde. Nucleus staining was conducted by DAPI; for this process, spheroids were kept immersed in 10 μM DAPI solution for 24 h. Finally, the spheroids were washed again with PBS, and then placed in a glass bottom dish with 90% glycerol. Micelle penetration in 3D cell aggregates was observed using CLSM using diode laser (405 nm) for DAPI, Ar-laser (458 nm/488 nm/514 nm) for epirubicin, and He—Ne laser (633 nm) for Alexa-647. Data processing was done as described above. To calculate the epirubicin fluorescence across the spheroids, data from 3 spheroids were averaged. For each spheroid, intensity profile across 10–12 cross-sectional lines at the 100 μm cross-sectional plane were averaged. Statistical significance was determined as mentioned above.

2.17. Animals and animal care

BALB/c-nu/nu mice (6 weeks old female with 18–20 g body weight at the start point of experiments) were purchased from Charles River Japan (Kanagawa, Japan). Animals were maintained in a temperature-controlled, sterile disease-free condition with a 12 h/12 h light/dark schedule. All animal experiments were performed in accordance with the guidelines for the care and use of laboratory animals as stated by the University of Tokyo and also ethics committee of the Innovation Center of NanoMedicine (Kawasaki, Japan).

2.18. In vivo antitumor activity study against orthotopic GBM model using U87MG-LUC

For the orthotopic tumor model, U87MG-Luc2 (1.0×10^5 cells in 2 μL injection volume) was transplanted intracranially at 1.0 mm anterior and 2.0 mm to the right side of the bregma and 3.0 mm deep in the brain surfaces of Balb/c nude mice. The tumors were allowed to grow for 5 to 6 days, and antitumor activity assay was initiated in 4 groups of BALB/c nude mice ($n = 8$). The groups were, PBS as control, free epirubicin 7 mg/kg, and the micelle groups (Epi/m and cRGD-Epi/m) with the dose was chosen to be of 15 mg/kg. Treatment schedule was set to 3 times injection at 3 days intervals (0, 4 and 8 days). *In vivo* imaging was done using an IVIS Spectrum (Xenogen Corporation) and D-Luciferin potassium salt solution was used as a substrate for lucifer-

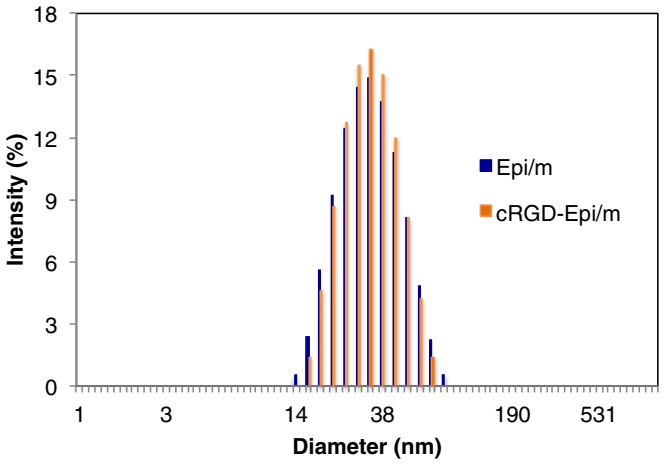

Fig. 2. Size of epirubicin-loaded micelles (Epi/m) and cRGD-installed Epi/m (cRGD-Epi/m). The intensity distribution of the diameter of the micelles was determined by DLS.

ase. Statistical significance was determined as mentioned earlier.

2.19. Tissue section preparation for histological examination

Tumor model was created according to the procedure described above. Brain section containing U87MG-GFP/U87MG-LUC tumor were collected 6 hour post intravenous injection of dye labeled micelle solution. Frozen brain tissue sections containing U87MG-GFP/U87MG-LUC embedded in OCT were cryo-sectioned (8 μm) using Leica CM1950 cryostat. The tissue slices were washed with PBS buffer, fixed with 4% paraformaldehyde and finally vectashield-mounting medium with DAPI was used to stain nucleus. Fixed and stained tissue sections were then imaged using CLSM.

3. Results

3.1. Polymer preparation and characterization

Acetal-poly(ethylene glycol)-*b*-poly(β-benzyl L-aspartate) (Acetal-PEG-*b*-PBLA; M_w of PEG = 12 kDa; polymerization degree of PBLA = 35) was synthesized, as the precursor polymer for the conjugation of cRGD peptide, by ring-opening polymerization of *β*-benzyl L-aspartate *N*-carboxyanhydride [32], initiated by the terminal primary amino group of α-acetal-ω-amino poly(ethylene glycol) (Scheme 1). The resulting block copolymer showed narrow and unimodal distribution of molecular weight, evident by GPC analysis (molecular weight distribution, M_w/M_n: 1.07). The degree of polymerization of the PBLA block was determined by comparing the peak intensity of the protons in β-benzyl residue (7–7.5 ppm) and PEG protons (−O−CH_2−CH_2−; 3.5 ppm) in the ^{1}H NMR spectrum. The six methyl-proton peaks of the acetal end group appeared as a well-resolved triplet at 1.1 ppm.

Prior to cRGD peptide conjugation at the α-end of acetal-PEG-*b*-PBLA polymer, the ω-amine functionality was terminated by acetylation. The complete protection of amine function was confirmed by ^{1}H NMR spectrum, where the acyl (CH_3CO−) proton peaks were compared with the methyl protons (2 × 3) of the acetal group and also two sets of methylene (−CH_2−) proton peaks of the PEG-PBLA polymer (Supplementary Fig. S1). Subsequently, cRGD peptide conjugation reaction was conducted through a one-pot acetal-deprotection and thiazolidine ring formation reaction (Scheme 1). Thus, the acetal group was acid-hydrolyzed to furnish an aldehyde function, which was then reacted with the cysteine moiety, attached to the cRGD peptide through a linker, to form the thiazolidine ring. Conjugation of cRGD peptide to furnish cRGD-PEG-PBLA-Ac was determined to be around 95% by ^{1}H NMR spectrum (Supplementary Fig. S2).

Specific units of hydrazide functions were introduced into the PEG-PBLA backbone according to our former work [33] to furnish poly (ethylene glycol)-*b*-poly(hydrazinyl-aspartamide), where benzyl esters of PBLA side chain were substituted to hydrazinyl by the ester-amide exchange (EAE) reaction using anhydrous hydrazine (0.5 equivalent to each BLA units) in dry dimethyl sulfoxide (DMSO). This specific reaction condition generally produces PEG-Poly(hydrazinyl-aspartamide) polymer with 15–20 hydrazide units and the rest of the benzyl esters of PEG-PBLA polymer gets hydrolyzed during the work-up procedure. For the preparation of cRGD-installed micelles (cRGD-Epi/m), a mixture (1:3) of cRGD-PEG-PBLA-Ac and MeO-PEG-PBLA-Ac polymer was used [25] (Fig. 1), and for the preparation of control micelle (Epi/m), only MeO-PEG-PBLA-Ac polymer was used for EAE reaction. Epi conjugation with the hydrazide polymer was done in dimethyl sulfoxide (DMSO) at 40 °C for 72 h.

3.2. Preparation and physicochemical characterization of Epi/m and cRGD-Epi/m

The drug-polymer conjugate in DMSO was dialyzed against methanol for 24 h to remove unbound drug and also for solvent-exchange. The resulting methanolic solution of drug-polymer conjugate was evaporated in a round bottom flask, which produces a thin film on the glass surface. PBS was then added and the mixture was subjected to sonication, which instantly produced micelle solution. The micelle solution was subjected to centrifugal ultrafiltration, with a membrane having 30,000 Da molecular weight cut off, to remove free polymer and to concentrate. Dynamic light scattering (DLS) measurements revealed narrowly distributed micellar-assemblies (Fig. 2) and identical diameter (30-nm) and polydispersity index (0.06) for both Epi/m and cRGD-Epi/m. Drug units conjugated per polymer chain of these micelle systems were calculated by correlating the drug concentration per milliliter micelle solution (determined by RPLC technique) with dry weight of polymer-drug conjugate (freeze-dried micelle solution) and it was found that the Epi/m and cRGD-Epi/m system contains 5 and 4 units of Epi per polymer chain, respectively (Table 1). In addition to size distribution and drug loading, Epi/m and cRGD-Epi/m demonstrated comparable pH-sensitivity for drug release when exposed to buffers with different pH, showing that drugs are rapidly discharged at acidic pH (Supplementary Fig. S3).

3.3. Cytotoxicity of free Epi, Epi/m and cRGD-Epi/m against U87MG 2D cell monolayer

The cytotoxic effect of the micelles was determined by evaluating the 50% growth inhibitory concentration (IC_{50}) against monolayer-cultured GBM cell line U87MG and compared with that of free Epi (Table 2). The IC_{50} values of both micelle systems were found to be comparable, when cells were exposed to micelle solutions for 3 h, washed and post-incubated for further 48 h. For the same experimental

Table 1
Diameter, polydispersity, polymer composition, hydrazide units per polymer chain, drug units per polymer chain, % drug loading of Epi/m and cRGD-Epi/m.

	Epi/m	cRGD-Epi/m
Diameter[a] (nm)	31	31
Polydispersity index	0.07	0.06
PEG-*b*-PBLA composition	12 K PEG 40 units PBLA	12 K PEG 40 units PBLA
Hydrazide units per polymer chain[b]	15	15
Epirubicin units per polymer chain[c]	5	4
% Drug loading (W/W)	14	12

[a] Determined by intensity% distribution obtained from DLS measurement.
[b] Determined by acetylation of hydrazide units and subsequent NMR analysis.
[c] Determined by HPLC and weight of dry Epi-polymer conjugate.

Table 2
Fifty-percent growth inhibitory concentration (IC_{50}) of free Epi, Epi/m and cRGD-Epi/m (n = 8 wells).

Drug exposure (h)	Post-incubation (h)	IC_{50}[a] (μg/mL)		
		Free Epi	Epi/m	cRGD-Epi/m
48	0	0.18	0.35	0.32
3	48	0.73	4.2	5.8

[a] Determined by MTT assay.

condition, the cytotoxicity of free Epi was found to be almost 7-fold higher than that of the micelles, may be due to rapid cellular and nuclear internalization ability of free drug (Supplementary Fig. S4), whereas micelle systems undergo gradual internalization through endocytosis and slow sustained release of Epi. In another cytotoxicity experiment, we continuously exposed the cancer cells to drugs for 48 h. The results indicated that the cytotoxic effect of both micelle systems was greatly enhanced and the IC_{50} value of free drug was only 2-fold lower than those of micelle systems, though there was no difference in the cytotoxicity of the micelles (Table 2).

3.4. Cell internalization study of micelles in monolayer U87MG cells

To better understand the cellular internalization kinetics of Epi/m and cRGD-Epi/m, we imaged the cells exposed with micelle solutions (3 μg/mL based on Epi concentration; this concentration was selected considering the cytotoxic data and visibility of Epi fluorescence under the imaging condition), for 1 h and 3 h, using confocal laser scanning microscopy (CLSM). The experimental results confirmed that although within the 3 h time frame cRGD-Epi/m almost evened out with Epi/m in terms of cellular internalization ability (intensity of Epi fluorescence), at the 1 h time point cRGD-Epi/m out-performed Epi/m almost 4-fold (Fig. 3b). This result implies a time dependent gradual internalization of Epi/m, probably through non-specific endocytosis. However, in case of cRGD-Epi/m, a fast internalization occurred at the early time point, which is presumably through integrin-mediated endocytosis. Interestingly, the internalization for cRGD-Epi/m at 3 h was not significantly higher than at 1 h, most probably due to cRGD-Epi/m reaching close to the saturation point within 1 h under the experimental condition.

3.5. Penetration of micelles in U87MG glioma spheroids.

Three-dimensional multi-cellular spheroids are generally considered as a more appropriate model than two-dimensional cell culture to envisage the *in vivo* response to therapeutics, as this model is intermediate in complexity between standard monolayer *in vitro* and tumors *in vivo* [28,34–37]. Three-dimensional spheroids replicate various aspects of the tumor microenvironment, such as gradients in oxygen, nutrient supply and pH [37]. More importantly, spheroids mimic the 3D multilayered cellular architecture with porosity and cell-cell network [38], which is specifically relevant to diffusive transport of nanoparticles and spatial distribution in tumor interstitium. Accordingly, we evaluated the biological characteristics of Epi micelles in 3D spheroid system. For this study, we used U87MG spheroids, cultured in non-adhesive U-bottom 96-well plates. The spheroid radius was maintained at approximately 100 μm to avoid necrosis in the center [28,35]. Spheroids were then treated with Epi, Epi/m and cRGD-Epi/m (equal concentration, 0.3 μg/mL of Epi; due to the multilayered structure of spheroids this concentration was found to be sufficient for Epi fluorescence visibility under the imaging condition) and CLSM imaging was performed after 3-, 6- and 24-h exposure to evaluate the penetration ability related to time of exposure (Fig. 4, Supplementary Fig. S5). The penetration ability of cRGD-Epi/m was found to be significantly superior in all measured time frames compared to that of Epi/m. A time-dependent enhancement in penetration was also obvious in case of cRGD-Epi/m, where intensity of Epi fluorescence increased in the

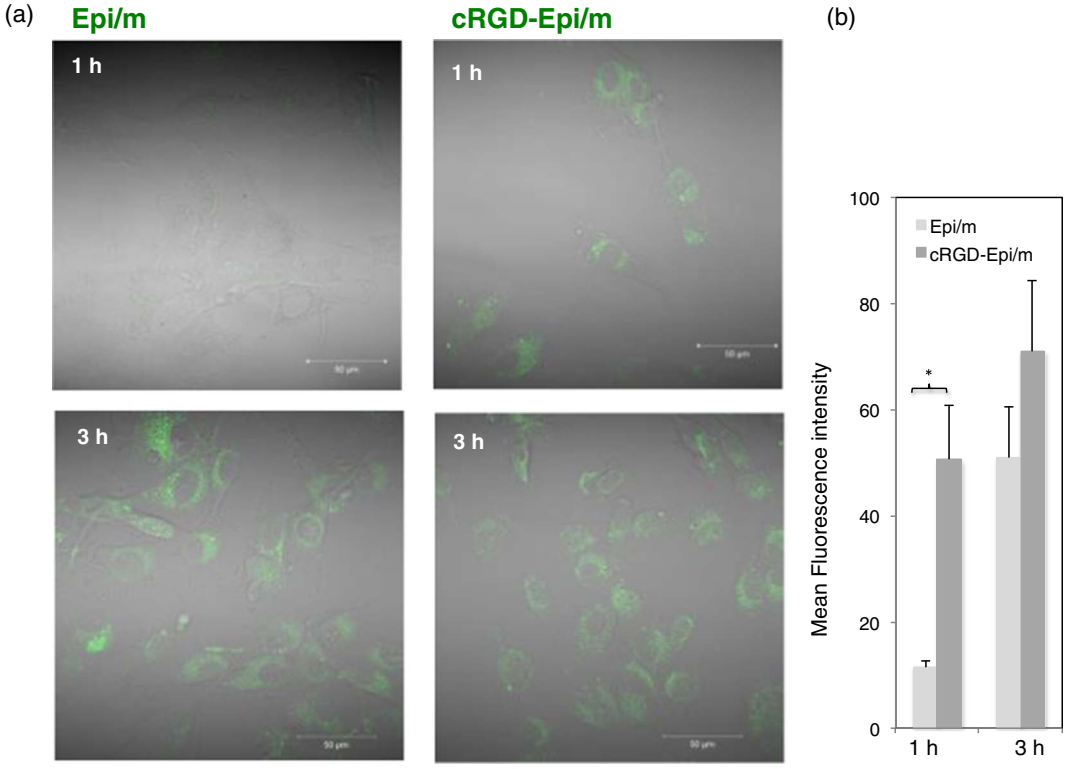

Fig. 3. Cell internalization study of epirubicin-loaded micelle (Epi/m) and cRGD-installed Epi/m (cRGD-Epi/m) in U87MG monolayer. (a) Intracellular distribution of epirubicin in the cells incubated with Epi/m (left) and cRGD-Epi/m (right) for 1 h (top) and 3 h (bottom). (b) Intensity profile of epirubicin fluorescence from Epi/m and cRGD-Epi/m (n = 3, $^*p < 0.0001$).

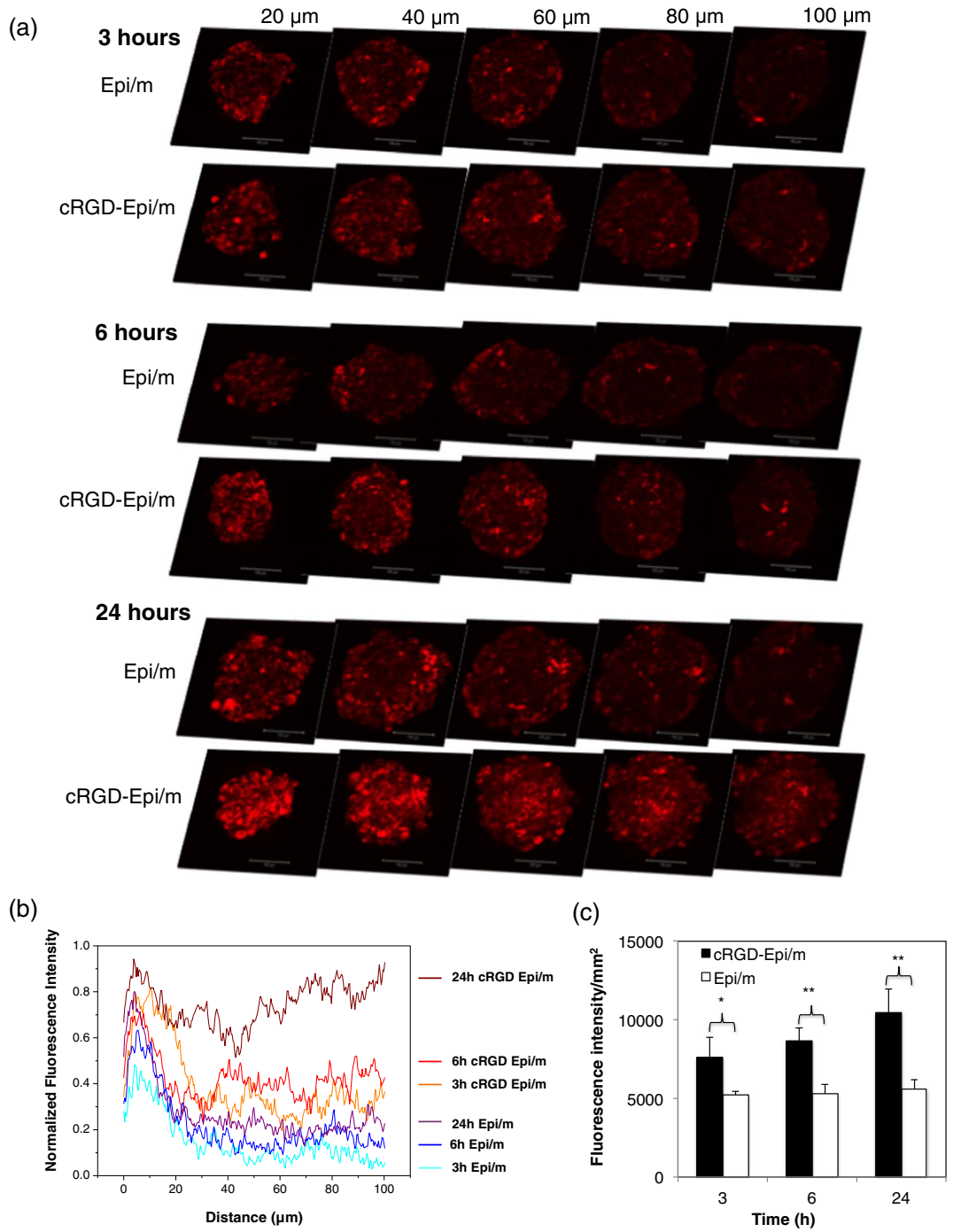

Fig. 4. Penetration of epirubicin-loaded micelles (Epi/m) and cRGD-installed Epi/m (cRGD-Epi/m) in U87MG spheroids. (a) *Z*-stack images of the spheroids were obtained by confocal laser scanning microscopy after incubation with the micelles for 3-, 6- and 24-h, starting from the top of the spheroids to 100 μm into the spheroids in intervals of 20 μm. Scale bars represent 100 μm. Red: Fluorescence from epirubicin. (b) Profile of epirubicin fluorescence across the spheroids at 3-, 6-, and 24-h normalized by the fluorescence intensity at the edge of the spheroid ($n = 3$). (c) Intensities of epirubicin fluorescence from Epi/m and cRGD-Epi/m at 100 μm cross-sectional slice for each spheroid ($n = 4$). Data expressed as the mean ± S.D. $^{*}p < 0.01$; $^{**}p < 0.0001$ by Student's *t*-test. (For interpretation of the references to colour in this figure legend, the reader is referred to the web version of this article.)

center part of spheroids with time. It is worth noting that the micelle concentration (0.3 μg/mL) for the imaging study was non-toxic for both Epi/m and cRGD-Epi/m against U87MG cells in 3D spheroid system after 24 h exposure; 100% cell survival was maintained even with 240 fold higher concentration than the IC_{50} determined in monolayer culture condition.

To further study the enhanced penetration of Epi from cRGD-Epi/m in the U87MG 3D spheroid, we labeled the micelles [31] with Alexa 647 and repeated the penetration study using CLSM after 24 h exposure with Alexa 647-labeled Epi/m (Alexa 647-Epi/m) and cRGD-Epi/m (Alexa 647-cRGD Epi/m). For this experiment, cells in the 3D spheroids were examined with higher magnification to observe the distribution of fluorescence-labeled micelles (green) and Epi (red) in the cellular level. The result of this study (Fig. 5a) reveals fluorescence intensity of Alexa 647 within green or yellow dot structures, in the cytoplasmic compartment of cells incubated with both Alexa 647-Epi/m and Alexa 647-cRGD-Epi/m micelle system, indicating an expected endocytosis mediated transport, and also presence of epirubicin fluorescence in the nuclear region (Fig. 5b) confirms the entry of released epirubicin (from both micelle systems). However, the obvious higher intensity and

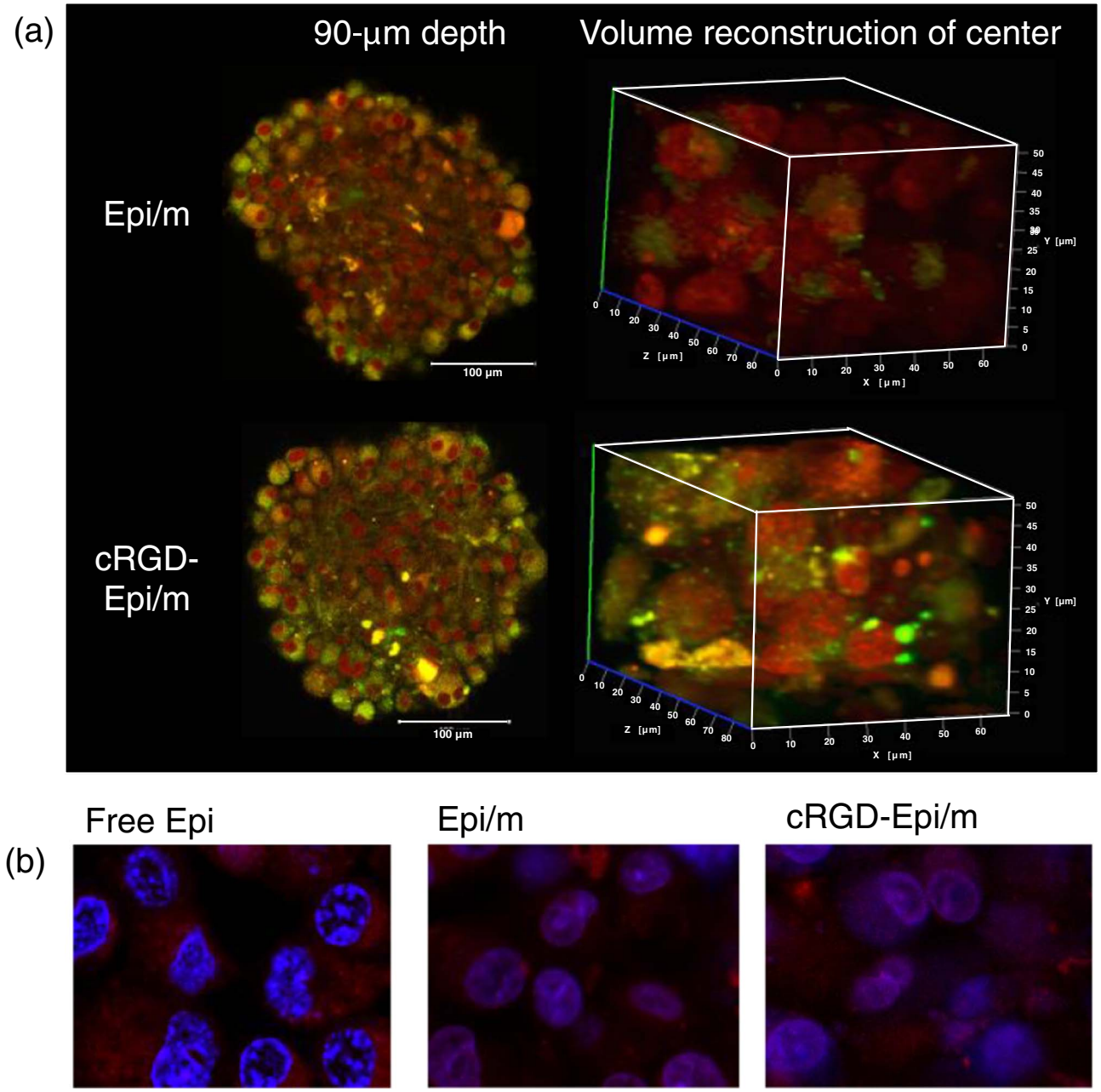

Fig. 5. Microdistribution of micelles and the delivered epirubicin inside U87MG spheroids. (a) The distribution of Alexa 647-labeled Epi/m and Alexa 647-labeled cRGD-Epi/m was observed by CLSM at 90-μm cross-sectional slice of U87MG spheroids (left panel), as well as by volume reconstruction through *Z*-stacking images from surface to 90-μm depth of spheroid parts after 24 h exposure (right panel). Green: Alexa 647, Red: epirubicin, Yellow: Colocalization of Alexa 647 and epirubicin. (b) Representing the micro-distribution of free epirubicin and released epirubicin from micelles inside cells after 24 h incubation with free Epi, Epi/m and cRGD/m. Red: epirubicin, Blue: DAPI, Purple: Colocalization of DAPI and epirubicin. (For interpretation of the references to colour in this figure legend, the reader is referred to the web version of this article.)

population of green and yellow dots in the cells incubated with Alexa 647-cRGD-Epi/m, than the ones incubated with Alexa 647-Epi/m, suggests higher population of Alexa 647-cRGD-Epi/m compare to that of Alexa 647-Epi/m. Interestingly in case of spheroids incubated with free epirubicin for 24 h, the distributions of the drug in the nucleus and in the cytosol were opposite to those of the micelle systems, as the fluorescence intensity at the cytoplasmic region was much higher than that in the nucleus (Fig. 5b and Supplementary Fig. S6).

3.6. In vivo antitumor activity studies against orthotopic U87MG-LUC tumors

For studying the antitumor activity *in vivo*, we implanted bioluminescent U87MG-lUC tumors in the brain of mice. The maximum tolerated dose was then used for both free drug (7 mg/kg) and the micelles (15 mg/kg), as previously reported [29,39] and also from our preliminary studies (body weight loss due to treatment of all groups was < 20%, which was determined to be the standard to choose MTD, data shown in Supplementary Fig. S7). Drugs were intravenously injected 3 times every 4th day, *i.e.* on days 0, 4, and 8 from the start of the experiment. Tumor growth progression was monitored, by measuring the bioluminescence intensity, using IVIS imaging system. While free Epi and Epi/m could not suppress the progression of the orthotopic xenografts (Fig. 6a), cRGD-Epi/m significantly reduced the growth of the tumors, showing a 12-fold lower photon flux than the group treated with Epi/m on day 21st after the start of treatment (Fig. 6a). Representative bioluminescent images from mice treated with PBS, Epi, Epi/m and cRGD-Epi/m at different time points clearly depict

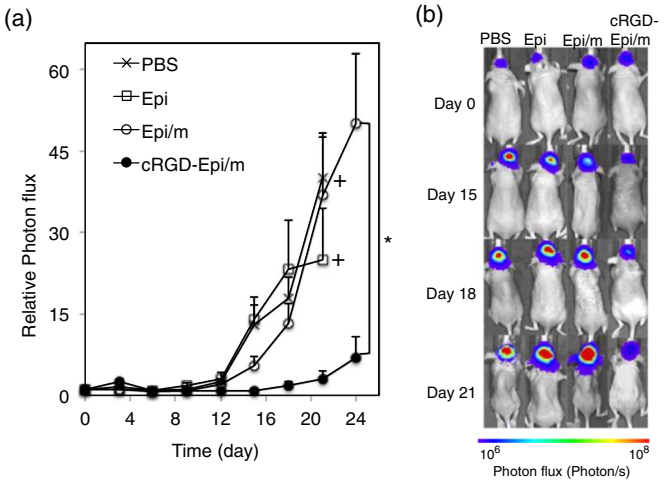

Fig. 6. Antitumor activity against bioluminescent orthotopic U87-MG-luc tumors. (a) Antitumor activity of free epirubicin (Epi) at 7 mg/kg, epirubicin-loaded micelles (Epi/m) at 15 mg/kg and cRGD-installed Epi/m (cRGD-Epi/m) at 15 mg/kg against U87MG-luc orthotopic tumor model. Drugs were injected 3 times every 4 days, on days 0, 4 and 8. Data are the mean ± S.D. ($n = 8$). *$p < 0.01$, Student's *t*-test, +: 3 of 8 mice dead. (b) Representative bioluminescence images of mice injected with PBS, Epi, Epi/m and cRGD-Epi/m at days 15, 18 and 21.

the substantial antitumor effect of cRGD-Epi/m (Fig. 6b). The superior antitumor effect of cRGD-Epi/m against orthotopic GBM tumor can be correlated with the effective penetration through BBTB, utilizing αvβ3/αvβ5 integrin mediated efficient transcellular transport [25]. Thus the accumulation of Epi/m and cRGD-Epi/m was investigated for examining the penetration efficacy of cRGD-Epi/m in the intracranial U87MG tumors.

3.7. Accumulation of fluorescent-labeled Epi/m and cRGD-Epi/m in orthotopic U87MG tumors

For this experiment, the core of Epi/m was labeled with Alexa 555 (Alexa 555-Epi/m) and that of cRGD-Epi/m was labeled with Alexa 647 (Alexa 647-cRGD-Epi/m). Both micelles were intravenously co-injected in mice bearing orthotopically implanted with U87MG cells expressing green fluorescence protein (U87MG-GFP). Concentrations of Alexa 555-Epi/m and Alexa 647-cRGD-Epi/m solutions for the intravenous co-injection were adjusted to have similar fluorescence intensity of both Alexa 555 and Alexa 647. Six-hours post injection; the brains having U87MG-GFP tumors were collected for CLSM examination. Results showed low fluorescence intensity for Alexa 555-Epi/m in the U87MG-GFP tumors (Fig. 7a), compared to Alexa 647-cRGD-Epi/m, suggesting poor penetration efficiency of the micelles without cRGD. To quantify the accumulation of fluorescent-labeled Epi/m and cRGD-Epi/m in orthotopic glioblastoma tumors, the experiment was repeated by using Epi/m and cRGD-Epi/m labeled with Alexa 647 at equivalent fluorescent intensity in separate sets of mice bearing orthotopic U87MG-LUC tumors ($n = 3$). Six-hours post injection, the tumor-bearing brains were collected for histological examination. The results showed almost 4-fold higher accumulation of Alexa-647-cRGD-Epi/m compared to Alexa-647-Epi/m (Fig. 7b, c), demonstrating significantly high localization of cRGD-Epi/m in the U87MG-LUC orthotopic tumor.

4. Discussion

Our results demonstrated significant antitumor effect of cRGD-Epi/m against orthotopic GBM, *i.e.* a 12-fold higher anti-tumor activity was displayed by cRGD-Epi/m than that of Epi/m. This efficacy enhancement correlated with the high tumor distribution of fluorescent-labeled cRGD-Epi/m in the orthotopic tumors, demonstrating the ability of these micelles for overcoming the BBB/BBTB in GBM. Such potency and capability indicate cRGD-Epi/m as an attractive therapeutic strategy against GBM.

The induction of transcellular-targeting of cRGD-Epi/m is evident in our 3D-spheroid penetration studies, where cRGD-Epi/m demonstrated superior efficacy to penetrate into deeper part of spheroids compared to Epi/m. As multicellular 3D spheroids deliver a valuable platform for studying nanomedicine behaviors in tumor tissue by mimicking *in vivo* tumor properties [40–42], the porosity and cell junctions in this *in vitro* model could pose significant obstacles for Epi/m migration and accumulation in the interior of spheroids. On the other hand, the rapid delivery of cRGD-Epi/m into deep parts of spheroids may be facilitated by their interaction with the integrins on cancer cells. A possible transcytosis pathway through cRGD-integrin mediated active transport [25,43] might be the driving force for enhanced penetration of cRGD-Epi/m, allowing the passage through the dense cellular layers. Such improved penetration mechanism of cRGD-Epi/m could enable supplying therapeutic doses to distant and poorly vascularized regions in tumors.

Integrins are associated with invasion and angiogenesis [44], the two crucial pathophysiological components of GBM. Integrin-mediated signaling pathways have been found to stimulate the tumor progression and metastasis by modifying the brain microenvironment to support the formation of the tumoral niche [45]. Integrins thus befits as one of the most auspicious molecules for targeted GBM therapy. The tripeptide sequence arginine-glycine-aspartic acid (RGD) found in many ECM proteins (such as fibronectin, vitronectin and collagens) is a well-established ligand for integrins such as αvβ3, αvβ5, and α5β1, and thus RGD peptides offer a promising approach for GBM therapy as a small molecule integrin antagonist (for example, Cilengitide [46]), alternatively [47] as an integrin-interactive motif for actively-targeted macromolecular delivery [45–47]. It is well demonstrated that tumor-associated blood vessels or neovasculatures has higher expression of integrins compare to normal blood vessels [48]. Given that GBM is angiogenesis-dependent, elevated tumor accumulation of RGD modified NPs is expected from the attachment with integrins expressed in GBM neovasculature, facilitating translocation from blood vessel to GBM site. Higher expression of integrins on U87 cells [49] would then aid greater association of RGD installed NPs with glioblastoma cells to enable effective internalization. Thus, RGD-binding integrins expressed in GBM neovasculature provide a counter-productive measure against the much inferior transvascular transport of NPs through the tight junction of BBTB related to the orthotopic brain tumor. In the present case, this cRGD-integrin mediated higher tumor accumulation and uptake was strategically coupled to effectively deliver, epirubicin, one of the most potent anti-glioblastoma agents, through pH-sensitive polymeric micelle for the successful treatment of GBM. Thus, the superior antitumor effect of cRGD-Epi/m against orthotopic GBM model compared to Epi/m can be attributed to αvβ3/αvβ5 integrin-mediated enhanced recognition and internalization to overcome BBTB, which ultimately attributed positively in the overall antitumor efficacy.

5. Conclusion

We have developed cRGD-installed polymeric micelles conjugating epirubicin through a pH-sensitive hydrazone-bond for effective treatment of GBM. These cRGD-Epi/m were effective against an orthotopic GBM model, achieving enhanced accumulation and penetration in the tumors. The high potency and ability to reach deep into the malignancies indicate cRGD-Epi/m as an attractive approach for treating GBM. Moreover, as Epi/m is already advancing in the clinical pipeline, the straightforward modification of their surface with cRGD peptide could potentially extend their clinical application as an effective brain tumor therapy.

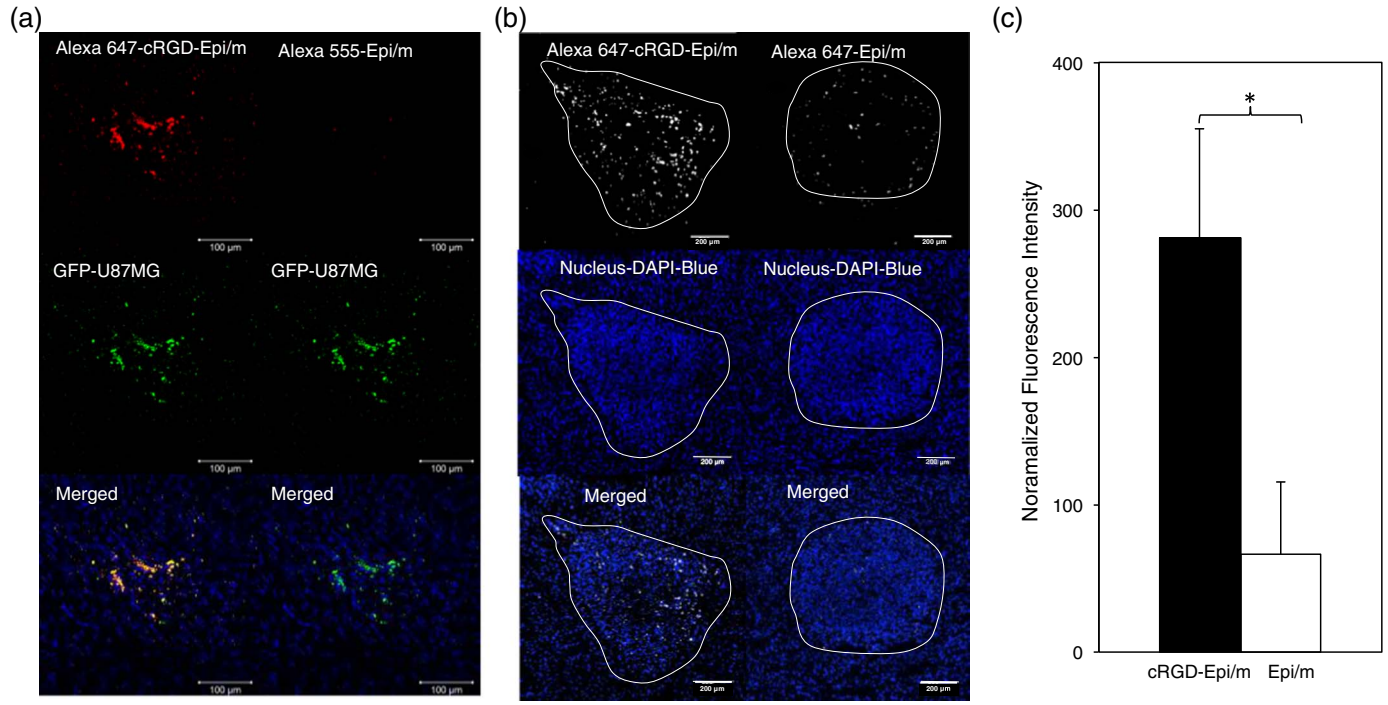

Fig. 7. Accumulation profile of fluorescent-labeled Epi/m and cRGD-Epi/m in orthotopic U87MG tumors. (a) Distribution of Alexa 555-labeled (red) epirubicin-loaded micelles (Alexa 555-Epi/m) and Alexa 647-labeled (red) cRGD-installed Epi/m (Alexa-647-cRGD-Epi/m) in U87MG-GFP cells implanted cranially. Blue: DAPI; Green: GFP; Red: Alexa 647 or Alexa 555. (b) Distribution of Alexa 647-labeled Epi/m and cRGD-installed Epi/m in U87MG-LUC cells implanted cranially. Blue: DAPI, White: Alexa 647. Tumor tissue fraction can be differentiated from normal tissue section by the nearness of cells distributed in a specific location (ROI in white) (c) Intensities of Alexa-647 fluorescence from Epi/m and cRGD-Epi/m distributed in orthotopically implanted U87MG-Luc cells ($n = 3$). Data was normalized by background (643 nm laser) fluorescence intensity/μm^2 in an U87MG-Luc brain tumor section collected from non-treated mice, $^*p = 0.014$ by Student's t-test. (For interpretation of the references to colour in this figure legend, the reader is referred to the web version of this article.)

Acknowledgements

This study was supported by the Center of Innovation (COI) Program from Japan Science and Technology Agency (JST), and Takeda Science Foundation. This research is partially supported by the Practical Research for Innovative Cancer Control from Japan Agency for Medical Research and Development, AMED, as well as Grants-in-Aid for Scientific Research (B; No. 16H03179 to H.C., No 16H05422 to Y. M), Grants-in-Aid for Young Scientists (A: No. 24689051 to Y. M), and Challenging Exploratory Research (No. 16K12904 to S.Q.)

Appendix A. Supplementary data

Supplementary data to this article can be found online at http://dx.doi.org/10.1016/j.jconrel.2017.04.033.

References

[1] E.C. Holland, Glioblastoma multiforme: the terminator, Proc. Natl. Acad. Sci. U. S. A. 97 (2000) 6242–6244.
[2] Y.P. Ramirez, J.L. Weatherbee, R.T. Wheelhouse, A.H. Ross, Glioblastoma multiforme therapy and mechanisms of resistance, Pharmaceutical 6 (2013) 1475–1506.
[3] A. Claes, A.J. Idema, P. Wesseling, Diffuse glioma growth: a guerilla war, Acta Neuropathol. 11 (2007) 443–458.
[4] R.K. Jain, E. di Tomaso, D.G. Duda, J.S. Loeffler, A.G. Sorensen, T.T. Batchelor, Angiogenesis in brain tumours, Nat. Rev. Neurosci. 8 (2007) 610–622.
[5] W.M. Pardridge, The blood-brain barrier: bottleneck in brain drug development, NeuroRx 2 (2005) 3–14.
[6] O. Van Tellingen, B. Yetkin-Arik, M.C. de Gooijer, P. Wesseling, T. Wurdinger, H.E. de Vries, Overcoming the blood-brain tumor barrier for effective glioblastoma treatment, Drug Resist. Updat. 19 (2015) 1–12.
[7] D. Khosla, Concurrent therapy to enhance radiotherapeutic outcomes in glioblastoma, Ann. Transl. Med. 4 (2016) 54.
[8] R.P. Thomas, L. Recht, S. Nagpal, Advances in the management of glioblastoma: the role of temozolomide and MGMT testing, Clin. Pharm. 5 (2013) 1–9.
[9] B. Daglar, E. Ozgur, M.E. Corman, L. Uzun, G.B. Demirel, Polymeric nanocarriers for expected nanomedicine: current challenges and future prospects, RSC Adv. 4 (2014) 48639–48659.
[10] E. Blanco, A. Hsiao, A.P. Mann, M.G. Landry, F. Meric-Bernstam, M. Ferrari, Nanomedicine in cancer therapy: innovative trends and prospects, Cancer Sci. 102 (2011) 1247–1252.
[11] N. Nishiyama, Y. Matsumura, K. Kataoka, Development of polymeric micelles for targeting intractable cancers, Cancer Sci. 107 (2016) 867–874.
[12] Y. Matsumura, H. Maeda, A new concept for macromolecular therapeutics in cancer chemotherapy: mechanism of tumoritropic accumulation of proteins and the antitumor agent smancs, Cancer Res. 46 (1986) 6387–6392.
[13] X. Wei, Z. Chen, M. Ying, W. Lu, Brain tumor-targeted drug delivery strategies, Acta Pharm. Sin. B 4 (2014) 193–201.
[14] G.F. Woodworth, G.P. Dunn, E.A. Nance, J. Hanes, H. Brem, Emerging insights into barriers to effective brain tumor therapeutics, Front. Oncol. 4 (2014) 1–14.
[15] Y. Matsumura, K. Kataoka, Preclinical and clinical studies of anticancer agent incorporating polymer micelles, Cancer Sci. 100 (2009) 572–579.
[16] H. Cabral, K. Kataoka, Progress of drug-loaded polymeric micelles into clinical studies, J. Control. Release 190 (2014) 465–476.
[17] W. Arap, R. Pasqualini, E. Ruoslahti, Cancer treatment by targeted drug delivery to tumor vasculature in a mouse model, Science 279 (1998) 377–380.
[18] R. Haubner, D. Finsinger, H. Kessler, Stereoisomeric peptide libraries and peptidomimetics for designing selective inhibitors of the $\alpha_v\beta_3$ integrin for a new cancer therapy, Angew. Chem. Int. Ed. Eng. 36 (1997) 1374–1389.
[19] E.F. Plow, T.A. Haas, L. Zhang, J. Loftus, J.W. Smith, Ligand binding to integrins, J. Biol. Chem. 275 (2000) 21785–21788.
[20] J.D. Humphries, A. Byron, M.J. Humphries, Integrin ligands at a glance, J. Cell Sci. 119 (2006) 3901–3903.
[21] S. Zitzmann, V. Ehemann, M. Schwab, Arginine-glycine-aspartic acid (RGD)-peptide binds to both tumor and tumor-endothelial cells in vivo, Cancer Res. 62 (2002) 5139–5143.
[22] R.H. Mattern, S.B. Read, M.D. Pierschbacher, C.I. Sze, B.P. Eliceiri, C.A. Kruse, Glioma cell integrin expression and their interactions with integrin antagonists, Cancer Ther. 3A (2005) 325–340.
[23] M.C. Gingras, E. Roussel, J.M. Bruner, C.D. Branch, R.P. Moser, Comparison of cell adhesion molecule expression between glioblastoma multiforme and autologous normal brain tissue, J. Neuroimmunol. 57 (1995) 143–153.
[24] S. Martin, H. Janouskova, M. Dontenwill, Integrins and p53 pathways in glioblastoma resistance to temozolomide, Front. Oncol. 2 (2012) 157 (eCollection).
[25] Y. Miura, T. Takenaka, K. Toh, S. Wu, H. Nishihara, M.R. Kano, Y. Ino, T. Nomoto, Y. Matsumoto, H. Koyama, H. Cabral, N. Nishiyama, K. Kataoka, Cyclic RGD-linked polymeric micelles for targeted delivery of platinum anticancer drugs to glioblastoma through the blood-brain tumor barrier, ACS Nano 7 (2013) 8583–8592.
[26] P. Jiang, R. Mukthavaram, Y. Chao, I.S. Bharati, V. Fogal, S. Pastorino, X. Cong, N. Nomura, M. Gallagher, T. Abbasi, S. Vali, S.C. Pingle, M. Makale, S. Kesari, Novel anti-glioblastoma agents and therapeutic combinations identified from a collection

of FDA approved drugs, J. Transl. Med. 12 (2014) 13.
[27] M.S. Lesniak, U. Upadhyay, R. Goodwin, B. Tyler, H. Brem, Local delivery of doxorubicin for the treatment of malignant brain tumors in rats, Anticancer Res. 25 (2005) 3825–3831.
[28] Y. Bae, S. Fukushima, A. Harada, K. Kataoka, Design of environment-sensitive supramolecular assemblies for intracellular drug delivery: polymeric micelles that are responsive to intracellular pH change, Angew. Chem. Int. Ed. 42 (2003) 4640–4643.
[29] A. Takahashi, Y. Yamamoto, M. Yasunaga, Y. Koga, J. Kuroda, M. Takigahira, M. Harada, H. Saito, T. Hayashi, Y. Kato, T. Kinoshita, N. Ohkohchi, I. Hyodo, Y. Matsumura, NC-6300, an epirubicin-incorporating micelle, extends the anti-tumor effect and reduces the cardiotoxicity of epirubicin, Cancer Sci. 104 (2013) 920–925.
[30] T. Bae, N. Nishiyama, S. Fukushima, H. Koyama, Y. Matsumura, K. Kataoka, Preparation and biological characterization of polymericmicelle drug carriers with intracellular pH-triggered drug release property: tumor permeability, controlled subcellular drug distribution, and enhanced in vivo antitumor efficacy, Bioconjug. Chem. 16 (2005) 122–130.
[31] S. Quader, H. Cabral, Y. Mochida, T. Ishii, X. Liu, K. Toh, H. Kinoh, Y. Miura, N. Nishiyama, K. Kataoka, Selective intracellular delivery of proteasome inhibitors through pH-sensitive polymeric micelles directed to effcient antitumor therapy, J. Control. Release 188 (2014) 67–77.
[32] M. Yokoyama, G.S. Kwon, T. Okano, Y. Sakurai, T. Seto, K. Kataoka, Preparation of micelle-forming polymer–drug conjugates, Bioconjug. Chem. 3 (1992) 295–301.
[33] Y. Bae, W.D. Jang, N. Nishiyama, S. Fukushima, K. Kataoka, Multifunctional polymeric micelles with folate-mediated cancer cell targeting and pH-triggered drug releasing properties for active intracellular drug delivery, Mol. BioSyst. 1 (2005) 242–250.
[34] L.A. Kunz-Schughart, Multicellular tumor spheroids; intermediates between monolayer culture and in vivo tumor, Cell Biol. Int. 23 (1999) 157–161.
[35] X. Xu, M.C. Farach-Carson, X. Jia, Three-dimensional in vitro tumor models for cancer research and drug evaluation, Biotechnol. Adv. 32 (2014) 1256–1268.
[36] G. Mehta, A.Y. Hsiao, M. Ingram, G.D. Luker, S. Takayama, Opportunities and challenges for use of tumor spheroids as models to test drug delivery and efficacy, J. Control. Release 164 (2012) 192–204.
[37] R.M. Sutherland, Cell and environment interactions in tumor micro regions: the multicell spheroid model, Science 240 (1988) 177–184.
[38] Y. Gao, M. Li, B. Chen, Z. Shen, P. Guo, M.G. Wientjes, J.L. Au, Predictive models of diffusive nanoparticle transport in 3-dimensional tumor cell spheroids, AAPS J. 15 (2013) 816–831.
[39] M. Harada, I. Bobe, H. Saito, N. Shibata, R. Tanaka, T. Hayashi, Y. Kato, Improved anti-tumor activity of stabilized anthracycline polymeric micelle formulation, NC-6300, Cancer Sci. 102 (2011) 192–199.
[40] T.T. Goodman, J. Chen, K. Matveev, S.H. Pun, Spatio-temporal modeling of nanoparticle delivery to multicellular tumor spheroids, Biotechnol. Bioeng. 101 (2008) 388–399.
[41] D. Loessner, K.S. Stok, M.P. Lutolf, D.W. Hutmacher, J.A. Clements, S.C. Rizzi, Bioengineered 3D platform to explore cell-ECM interactions and drug resistance of epithelial ovarian cancer cells, Biomaterials 31 (2010) 8494–8506.
[42] G. Fracasso, M. Colombatti, Effect of therapeutic macromolecules in spheroids, Crit. Rev. Oncol. Hematol. 36 (2000) 159–178.
[43] X. Jiang, X. Sha, H. Xin, X. Xu, J. Gu, W. Xia, S. Chen, Y. Xie, L. Chen, Y. Chen, X. Fang, Integrin-facilitated transcytosis for enhanced penetration of advanced gliomas by poly(trimethylene carbonate)-based nanoparticles encapsulating paclitaxel, Biomaterials 34 (2013) 2969–2979.
[44] R. Max, R. Gerritsen, P. Nooijen, S.L. Goodman, A. Sutter, U. Keilholz, D.J. Ruiter, R. Dewall, Immunohistochemical analysis of integrin αvβ3 expression on tumor-associated vessels of human carcinomas, Int. J. Cancer 71 (1997) 320–324.
[45] M. Paolillo, M. Serra, S. Schinelli, Integrins in glioblastoma: still an attractive target? Pharm. Res. 113 (2016) 55–61.
[46] D.A. Reardon, B. Neyns, M. Weller, J.C. Tonn, L.B. Nabors, R. Stupp, Cilengitide: an RGD pentapeptide αvβ3 and αvβ5 integrin inhibitor in development for glioblastoma and other malignancies, Future Oncol. 7 (2011) 339–354.
[47] K. Chen, X. Chen, Integrin targeted delivery of chemotherapeutics, Theranostics 1 (2011) 189–200.
[48] J. Desgrosellier, D. Cheresh, Integrins in cancer: biological implications and therapeutic opportunities, Nat. Rev. Cancer 10 (2010) 9–22.
[49] L. Bello, M. Francolini, P. Marthyn, J. Zhang, R.S. Carroll, D.C. Nikas, J.F. Strasser, R. Villani, D.A. Cheresh, P.M. Black, Alpha(v)beta3 and alpha(v)beta5 integrin expression in glioma periphery, Neurosurgery 49 (2001) 380–389.